Acta Crystallographica Section F
Structural Biology and Crystallization Communications
ISSN 1744-3091

Purification, crystallization and preliminary X-ray diffraction of human S100A15

Karen M. Boeshans,[a] Ronald Wolf,[b] Christopher Voscopoulos,[b] William Gillette,[c] Dominic Esposito,[c] Timothy C. Mueser,[d] Stuart H. Yuspa[b] and Bijan Ahvazi[a]*

[a]X-ray Crystallography Facility, NIAMS, National Institutes of Health, Bethesda, MD 20892, USA, [b]Center for Cancer Research, National Cancer Institute, National Institutes of Health, Bethesda, MD 20892, USA, [c]Protein Expression Laboratory, Research Technology Program, National Cancer Institute, SAIC-Frederick Inc., Frederick, MD 21702, USA, and [d]Department of Chemistry, University of Toledo, Toledo, OH 43606, USA

Correspondence e-mail: ahvazib@mail.nih.gov

Received 22 February 2006
Accepted 8 April 2006

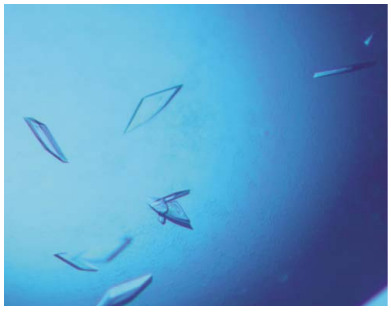

Human S100A15 is a novel member of the S100 family of EF-hand calcium-binding proteins and was recently identified in psoriasis, where it is significantly upregulated in lesional skin. The protein is implicated as an effector in calcium-mediated signal transduction pathways. Although its biological function is unclear, the association of the 11.2 kDa S100A15 with psoriasis suggests that it contributes to the pathogenesis of the disease and could provide a molecular target for therapy. To provide insight into the function of S100A15, the protein was crystallized to visualize its structure and to further the understanding of how the many similar calcium-binding mediator proteins in the cell distinguish their cognate target molecules. The S100A15 protein has been cloned, expressed and purified to homogeneity and produced two crystal forms. Crystals of form I are triclinic, with unit-cell parameters $a = 33.5$, $b = 44.3$, $c = 44.8$ Å, $\alpha = 71.2$, $\beta = 68.1$, $\gamma = 67.8^\circ$ and an estimated two molecules in the asymmetric unit, and diffract to 1.7 Å resolution. Crystals of form II are monoclinic, with unit-cell parameters $a = 82.1$, $b = 33.6$, $c = 52.2$ Å, $\beta = 128.2^\circ$ and an estimated one molecule in the asymmetric unit, and diffract to 2.0 Å resolution. This structural analysis of the human S100A15 will further aid in the phylogenic comparison between the other members of the S100 protein family, especially the highly homologous paralog S100A7.

1. Introduction

The S100 proteins comprise a family of 9–13 kDa calcium-binding proteins (Volz *et al.*, 1993). 16 S100 genes are located within the epidermal differentiation complex on human chromosome 1q21. S100 proteins are characterized by the presence of two distinct calcium-binding EF-hand motifs. They display different affinities for Ca^{2+} ions, having a canonical calcium-binding loop containing 12 amino acids and an N-terminal noncanonical calcium-binding motif that includes 14 amino acids that has a lower calcium affinity (Krebs *et al.*, 1995; Schäfer *et al.*, 1995; Heizmann & Cox, 1998). Of the 21 S100 proteins that have been cloned to date, 11, including S100A2, S100A3, S100A4, S100A6, S100A7, S100A8, S100A9, S100A10, S100A11, S100A12 and S100A15, are expressed in the human epidermis or in cultured keratinocytes (Eckert *et al.*, 2004); of these, seven structures have been solved (Mittl *et al.*, 2002; Otterbein *et al.*, 2002; Brodersen *et al.*, 1998; Itou *et al.*, 2002; Rety *et al.*, 1999, 2000; Moroz *et al.*, 2001). The recently identified S100A15 protein has the highest sequence identity of 93% to its paralog S100A7, followed by lower levels of identity to S100A11 (34%) and S100A8 (29%) (Wolf *et al.*, 2003). These related structures suggest that both EF-hands in S100A15 are flanked by hydrophobic regions at either terminus and are separated by a central hinge region with significant amino-acid sequence divergence within the family (Schäfer & Heizmann, 1996). In S100 proteins, the N-terminal EF-hand is rich in basic amino acids and the C-terminal EF-hand is rich in acidic amino acids within the canonical Ca^{2+}-binding loop common to all EF-hand Ca^{2+}-binding proteins. The large variation in the Ca^{2+}-binding affinities of the N- and C-terminal EF-hands indicate that S100 proteins engage in multiple functions in a wide variety of cell types and tissues (Krebs *et al.*, 1995; Hilt & Kligman, 1991). Zn^{2+} ions can replace and affect the binding of Ca^{2+} in particular S100 proteins, which further contributes

to their variable cation-binding properties and their diversified functions (Brodersen *et al.*, 1998; Baudier & Gerard, 1983) and divalent zinc should be considered a major regulator of their function (Filipek *et al.*, 1990; Föhr *et al.*, 1995; Leung *et al.*, 1987; Raftery *et al.*, 1996). It has been postulated that some S100 proteins such as S100A7 are zinc-regulated, based on the observation that zinc can be lost without denaturation of the protein (Baudier & Gerard, 1983; Baudier *et al.*, 1986). The amino-acid sequence of the Zn-binding motif of S100A15 is similar to those of other members of the S100 family such as S100A7, S100A9 and S100A12 in both the position and type of amino acids. It is most likely that S100A15 contains high-affinity zinc sites such as that in S100A7 despite the D24G substitution in S100A15 (Baudier & Gerard, 1983).

The S100 proteins exist in cells as heterodimers and homodimers and upon calcium binding interact with target proteins to regulate cell function (Sastry *et al.*, 1998). Identifying S100 intracellular distribution, site of action and protein targets remain important goals. The S100 proteins are mediators of calcium-associated signal transduction and undergo changes in subcellular distribution in response to extracellular stimuli (Eckert *et al.*, 2004). Some members function as chemotactic agents (Hoffmann *et al.*, 1994; Jinquan *et al.*, 1996) and may play a role in the pathogenesis of skin diseases, as selected S100 proteins are markedly overexpressed in psoriasis, wound healing, skin cancer, inflammation, cellular stress and other epidermal states (Broome *et al.*, 2003; Semprini *et al.*, 2002; Touitou *et al.*, 2002; Kerkhoff *et al.*, 1999; Broome & Eckert, 2004). Normal biological activity includes forming complexes with target proteins to modify function, involvement in membrane remodeling that occurs during keratinocyte differentiation, especially in reorganizing the keratinocyte surface, and function in the formation of calcium channels to facilitate the transmembrane influx of calcium that occurs during terminal differentiation (Hoffmann *et al.*, 1994). These proteins are also efficient transglutaminase substrates. The S100 proteins are incorporated into the cornified envelope by a transglutaminase-dependent covalent modification and may help protect against bacterial infection (Eckert *et al.*, 2004).

Little is presently known regarding the function of S100A15. Compared with normal epidermis, S100A15 mRNA levels are slightly increased in non-lesional and markedly increased in lesional psoriasis, where it was originally identified (Wolf *et al.*, 2003). In order to better understand its role in disease progression, we have cloned, expressed and purified the S100A15 protein to homogeneity and crystallized the S100A15 protein in two different crystal forms.

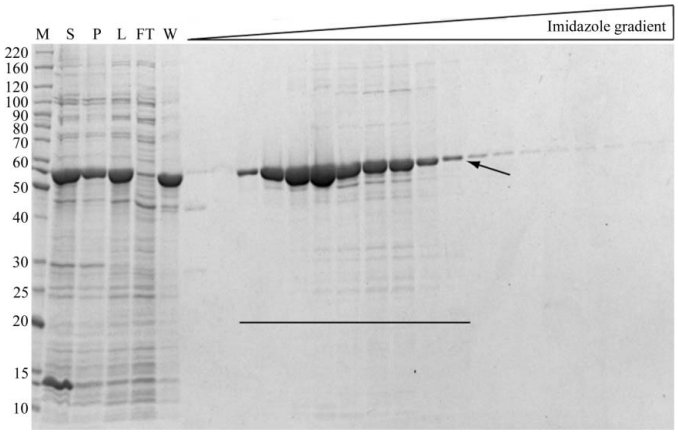

Figure 1
Purification of S100A15 protein. The protein sample was separated by 4–12% SDS–PAGE as shown for the following stages of purification, extraction and IMAC. M, protein standards (kDa); S, starting sample; P, insoluble fraction; L, column load; FT, flowthrough fraction; W, wash fraction. Arrows denote the location of his6-MBP-A15. The solid line indicates the fractions combined to prepare sample pools.

2. Synthesis of cDNAs and cloning of S100A15

Total RNA (1 µg) from psoriatic skin was denatured at 343 K for 10 min and first-strand cDNA was synthesized in a 20 µl reaction solution containing 4 µl 5× RT buffer (Invitrogen), 25 ng µl^{-1} oligo-dT primers, 0.5 m*M* dNTPs, 10 m*M* dithiothreitol (DTT), 40 U RNasin (Promega) and 200 U Superscript II-Reverse Transcriptase (Invitrogen) at 315 K for 1 h and 333 K for 10 min. For amplification of the S100A15-specific transcripts, PCR reactions were carried out in a total volume of 20 µl containing 1 µl of the RT sample, 2 µl 10× buffer (Qiagen), 1.5 m*M* $MgCl_2$, 0.2 m*M* dNTPs, DEPC-treated water and 2 U Taq polymerase (Qiagen) and 0.1 µ*M* of specific intron spanning primer pairs based on GenBank sequences (genomic clone RP1-128L15, accession No. AL591704; partial RNA hNICE, accession No. AJ243672), S100A15 isoform (NCBP5F sense 5′-CAAGTTCCTTCTGCTCCATCTTAG-3′, NCBP4R antisense 5′-GATTGTCTTTATTTCCTGAAGGCT-3′). The PCR temperature profile consisted of 31 cycles at 367 K for 1 min, 329 K for 1 min and 345 K for 1 min (time increment of 2 s per cycle) followed by an additional extension step at 345 K for 5 min. The PCR product was separated on a 1.5% agarose gel, extracted (QiaexII, Qiagen) and cloned into pCRII-TOPO (Invitrogen).

3. Expression and purification

Expression of all constructs was performed using *Escherichia coli* BL21 (DE3) cells harboring plasmid his6-MBP-tev-A15. Cells were incubated overnight at 310 K in LB medium containing ampicillin (50 µg ml^{-1}). This pre-culture was used to inoculate 4 l fresh LB ampicillin medium, which was incubated at 310 K until an optical density at 595 nm (OD_{595}) of approximately 0.5 was reached. Protein expression was induced with 0.5 m*M* IPTG and cells were incubated for an additional 4 h at 289 K. Cells were harvested by centrifugation, washed once with 2× PBS pH 7.2 and stored at 193 K. The *E. coli* cell paste was thawed and resuspended with 20 ml per gram wet weight of extraction buffer (20 m*M* sodium phosphate buffer pH 7.5, 100 m*M* NaCl, 5 m*M* $MgCl_2$, 5% glycerol, 1 m*M* βME, 45 m*M* imidazole) and one tablet of Complete protease inhibitor (Roche), digested with lysozyme (0.5 mg ml^{-1}) for 30 min on ice and treated with 10 U ml^{-1} benzonase for an additional 20 min. The sample was sonicated to lyse the cells (Branson sonifier 250, 100% power, 33% duty cycle for 3 × 20 s with a 1 cm tip), adjusted to a final concentration of 500 m*M* NaCl, clarified by centrifugation at 111 000*g* for 30 min, filtered (0.45 mm, PES membrane) and applied onto an IMAC column (5 ml HisTrap, GE Healthcare) equilibrated with binding buffer (extraction buffer with 500 m*M* NaCl). The column was first washed with binding buffer to baseline and proteins were eluted over a 20 column volume gradient (0–400 m*M* imidazole in binding buffer); fractions were analyzed by SDS–PAGE. The pool created from the IMAC fractions was dialyzed against binding buffer and treated with TEV protease for 60 min at RT and overnight at 277, 289, 298 and 303 K and analyzed by SDS–PAGE. The protease digestion was scaled up based on the results of the test digests. A second IMAC run was used to purify the target protein away from the contaminants of the protease digest. The elution was divided into two portions, a 0–50 m*M* imidazole-gradient sample over ten column volumes and a 50–400 m*M* imidazole-gradient sample over ten column volumes, and then analyzed by SDS–PAGE. Samples containing the S100A15

Table 1
Crystallographic parameters and data-processing statistics.

Values in parentheses are for the highest resolution shell.

Crystal form	I (triclinic)	II (monoclinic)
Space group	*P*1	*C*2
Unit-cell parameters (Å, °)	a = 33.5, b = 44.3, c = 44.8, α = 71.2, β = 68.1, γ = 67.8	a = 82.1, b = 33.6, c = 52.2, β = 128.2
Resolution range (Å)	50–1.70 (1.76–1.70)	30–2.0 (2.07–2.00)
Completeness (%)	90.2 (86.9)	95.7 (89.6)
Total reflections	425491	385258
Unique reflections	21586	6883
Overall $I/\sigma(I)$	14.6 (2.9)	18.1 (4.5)
$R_{\rm merge}$	0.067 (0.333)	0.072 (0.247)

protein were dialyzed (2 × 4 h at 277 K, 20 sample volumes of final buffer, 3500 MWCO Pierce Snakeskin dialysis membrane) and concentrated (3500 MWCO Amicon Ultra filtration device, Millipore). All gel samples were prepared using 4× LDS sample buffer (Invitrogen) and 20× TCEP reducing agent (BioRad). Samples were heated at 343 K for 5 min prior to application to Criterion Tris-glycine 10–20% pre-cast gels (BioRad). Proteins were visualized using 0.005% Coomassie Brilliant Blue R-250 in 0.3%(*v*/*v*) acetic acid. Where applicable, equal percentages of load, flowthrough and wash fractions were analyzed as shown in Fig. 1.

4. Crystallization and X-ray data collection

Initial crystallization attempts were made using Crystal Screens 1 and 2 (Hampton Research, Aliso Viejo, CA, USA). Trials were performed using the hanging-drop vapor-diffusion method at 277 K using VDX 24-well plates (Hampton Research) with 750 µl reservoir solution in each well. The drop contained 2 µl protein solution (7.5 mg ml^{-1}) in 20 m*M* Tris–HCl pH 8.0, 20 m*M* NaCl, 2 m*M* $CaCl_2$ and an equal volume of precipitant. Triangular plate-shaped crystals appeared after 1 d in 10 m*M* $ZnSO_4{\cdot}7H_2O$, 100 m*M* Na MES pH 6.5 and 25%(*v*/*v*) PEG monomethyl ether 550. The crystals from the initial screen were sufficient and no further optimization trials were performed to improve the crystal morphology. The crystals grew to dimensions of 150 × 100 × 75 µm within 48 h (Fig. 2) and were harvested into reservoir solution containing 30% ethylene glycol as a cryoprotectant with a rayon mounting loop (Hampton Research) and flash-frozen in a liquid nitrogen stream (Oxford Cryosystems, Oxford, England) prior to data collection. Initial X-ray diffraction data were tested in-house using an R-AXIS IV^{++} imaging-plate detector mounted on an RU-200 Rigaku rotating-anode X-ray generator with an Osmic mirror system operating at 50 kV and 100 mA. X-ray diffraction data from the crystals of S100A15 were collected on a MAR 300 detector at the Southeast Regional Collaborative Access Team (SER-CAT) 22-ID beamline at the Advanced Photon Source, Argonne National Laboratory. A crystal-to-detector distance of 200 mm, an oscillation range of 1.0° and an exposure of 2 s were used. In order to obtain highly redundant data from the crystal, 360° oscillation images ($\Delta\varphi$ = 1.0°) were obtained. The diffraction data was indexed, processed, scaled and merged using *HKL*2000 (Otwinowski & Minor, 1997). The real resolution of the data used for structure refinement was estimated by taking into consideration the completeness of the last resolution shell, the $I/\sigma(I)$ ratio and $R_{\rm merge}$ values. Data-collection statistics for the two crystal forms are summarized in Table 1.

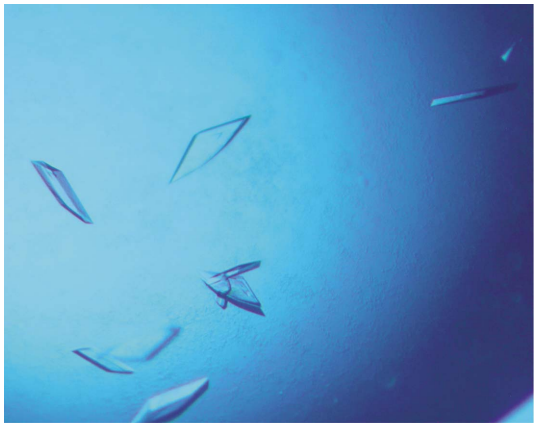

Figure 2
The crystal morphology of the S100A15 protein is shown. No attempt was made to optimize the crystal size and morphology. The initial crystallization screen leads to crystals with the same morphology but two different space groups that coexist in the same drop.

5. Discussion

We have cloned, expressed and purified the S100A15 protein to homogeneity. The novel psoriasis-associated gene S100A15 is unique in genomic organization among the S100 family, leading to alternative splice variants. The characterization of S100A15 will result in further insight into the regulation of the S100 genes. The novel S100A15 gene, encoding a protein with two Ca^{2+}-binding EF-hand motifs, is likely to participate in calcium homeostasis in the skin and might therefore be an important factor for proliferation and differentiation in psoriasis and other diseases. The recently identified S100A15 protein is structurally and functionally similar to human S100A7 (Brodersen *et al.*, 1998). The S100A7 protein is abundant in many human cell types, but most remarkably was found to be upregulated fivefold in the keratinocytes of patients suffering from the chronic and hyperproliferative skin disease psoriasis (Eckert *et al.*, 2004). In addition, S100A7 is implicated as the principal *E. coli* killing antimicrobial protein of healthy human skin and plays a putative role in tumor progression (Glaser *et al.*, 2005; Webb *et al.*, 2005).

S100A15 has been grown in two different crystal forms. The same crystallization and growth conditions lead to two different space-group crystals, which coexist in the same drop. The presence of zinc sulfate in the crystallization condition proved to be essential for formation of crystals of both S100A15 (triangular plate shaped) and S100A7 (bipyramidal shaped) (Nolsøe *et al.*, 1997). According to Matthews coefficient calculations (Matthews, 1968), a solvent content of 51.3% corresponds to the presence of two monomers in the asymmetric unit for the triclinic crystal form I. The crystals of form II are monoclinic and have a solvent content of 51.8%, corresponding to the presence of one monomer in the asymmetric unit. This suggests that the molecular dyad is aligned with a crystallographic axis in the *C*2 crystal form. We expect that the three-dimensional structure of S100A15 protein, while similar to the S100A7 protein (Brodersen *et al.*, 1998, 1999), will provide essential information about the molecular function and structural variations within the S100 family of proteins.

We are grateful to Dr Zbigniew Dauter for assistance with data collection on beamline 22-ID at the Advanced Photon Source, Argonne National Laboratory. The use of the Advanced Photon Source was supported by the US Department of Energy, Office of Science, Office of Basic Energy Sciences under Contract No. W-31-

109-Eng-38. RW is funded by the German Research Foundation (DFG), Emmy-Noether Program (Wo 843/2-1). CV is funded by a National Cancer Institute pre-doctoral research fellowship and by Tulane University School of Medicine. This research was supported in part by the Intramural Research Program of the National Institute of Arthritis and Musculoskeletal and Skin Diseases and National Cancer Institute, Center for Cancer Research of the National Institutes of Health.

References

Baudier, J. & Gerard, D. (1983). *Biochemistry*, **22**, 3360–3369.
Baudier, J., Glasser, N. & Gerard, D. (1986). *J. Biol. Chem.* **261**, 8192–8203.
Brodersen, D. E., Etzerodt, M., Madsen, P., Celis, J. E., Thogersen, H. C., Nyborg, J. & Kjeldgaard, M. (1998). *Structure*, **6**, 477–489.
Brodersen, D. E., Nyborg, J. & Kjeldgaard, M. (1999). *Biochemistry*, **38**, 1695–1704.
Broome, A. M. & Eckert, R. L. (2004). *J. Invest. Dermatol.* **122**, 29–38.
Broome, A. M., Ryan, D. & Eckert, R. L. (2003). *J. Histochem. Cytochem.* **51**, 675–685.
Eckert, R., Broome, A.-M., Ruse, M., Robinson, N., Ryan, D. & Lee, K. (2004). *J. Invest. Dermatol.* **123**, 23–33.
Filipek, A., Heizmann, C. W. & Kuznicki, J. (1990). *FEBS Lett.* **264**, 263–266.
Föhr, U. G., Heizmann, C. W., Engelkamp, D., Schäfer, B. & Cox, J. A. (1995). *J. Biol. Chem.* **270**, 21056–21061.
Glaser, R., Harder, J., Lange, H., Bartels, J., Christophers, E. & Schroder, J. M. (2005). *Nature Immunol.* **6**, 57–64.
Heizmann, C. W. & Cox, J. A. (1998). *Biometals*, **11**, 383–397.
Hilt, D. C. & Kligman, D. (1991). *Novel Ca^{2+}-binding Proteins: Fundamentals and Clinical Implications*, edited by C. W. Heizmann, pp. 65–103. Berlin: Springer Verlag.
Hoffmann, H. J., Olsen, E., Etzerodt, M., Madsen, P., Thogersen, H. C., Kruse, T. & Celis, J. E. (1994). *J. Invest. Dermatol.* **103**, 370–375.
Itou, H., Yao, M., Fujita, I., Watanabe, N., Suzuki, M., Nishihira, J. & Tanaka, I. (2002). *J. Mol. Biol.* **316**, 265–276.
Jinquan, T., Vorum, H., Larsen, C. G., Madsen, P., Rasmussen, H. H., Gesser, B., Etzerodt, M., Honore, B., Celis, J. E. & Thestrup-Pedersen, K. (1996). *J. Invest. Dermatol.* **107**, 5–10.
Kerkhoff, C., Klemp, M., Kaever, V. & Sorg, C. (1999). *J. Biol. Chem.* **274**, 32672–32679.
Krebs, J., Quadroni, M. & Van Eldik, I. J. (1995). *Nature Struct. Biol.* **2**, 711–714.
Leung, I. K. M., Mani, R. S. & Kay, C. M. (1987). *FEBS Lett.* **214**, 35–40.
Matthews, B. W. (1968). *J. Mol. Biol.* **33**, 491–497.
Mittl, P. R., Fritz, G., Sargent, D. F., Richmond, T. J., Heizmann, C. W. & Grutter, M. G. (2002). *Acta Cryst.* D**58**, 1255–1261.
Moroz, O. V., Antson, A. A., Murshudov, G. N., Maitland, N. J., Dodson, G. G., Wilson, K. S., Skibshoj, I., Lukanidin, E. M. & Bronstein, I. B. (2001). *Acta Cryst.* D**57**, 20–29.
Nolsøe, S., Thirup, S., Etzerodt, M., Thøgersen, H. C. & Nyborg, J. (1997). *Acta Cryst.* D**53**, 119–121.
Otterbein, L. R., Kordowska, J., Witte-Hoffmann, C., Wang, C. L. & Dominguez, R. (2002). *Structure*, **10**, 557–567.
Otwinowski, Z. & Minor, W. (1997). *Methods Enzymol.* **276**, 307–326.
Raftery, M. J., Harrison, C. A., Alewood, P., Jones, A. & Geczy, C. L. (1996). *Biochem. J.* **316**, 285–293.
Rety, S., Osterloh, D., Arie, J. P., Tabaries, S., Seeman, J., Russo-Marie, F., Gerke, V. & Lewit-Bentley, A. (2000). *Structure Fold. Des.* **8**, 175–184.
Rety, S., Sopkova, J., Renouard, M., Osterloh, D., Gerke, V., Tabaries, S., Russo-Marie, F. & Lewit-Bentley, A. (1999). *Nature Struct. Biol.* **6**, 89–95.
Sastry, M., Ketchem, R. R., Crescenzi, O., Weber, C., Lubienski, M. J., Hidaka, H. & Chazin, W. J. (1998). *Structure*, **6**, 223–231.
Schäfer, B. W. & Heizmann, C. W. (1996). *Trends Biochem. Sci.* **21**, 134–140.
Schäfer, B. W., Wicki, R., Engelkamp, D., Mattei, M. G. & Heizmann, C. W. (1995). *Genomics*, **25**, 638–643.
Semprini, S., Capon, F., Tacconelli, A., Giardina, E., Orecchia, A., Mingarelli, R., Gobello, T., Zambruno, G., Botta, A., Fabrizi, G. & Novelli, G. (2002). *Hum. Genet.* **111**, 310–313.
Touitou, E., Godin, B., Karl, Y., Bujanover, S. & Becker, Y. (2002). *J. Control. Release*, **80**, 1–7.
Volz, A., Korge, B. P., Compton, J. G., Ziegler, A., Steinert, P. M. & Mischke, D. (1993). *Genomics*, **18**, 92–99.
Webb, M., Emberley, E. D., Lizardo, M., Alowami, S., Qing, G., Alfia'ar, A., Snell-Curtis, L. J., Niu, Y., Civetta, A., Myal, Y., Shiu, R., Murphy, L. C. & Watson, P. H. (2005). *BMC Cancer*, **17**, 5–17.
Wolf, R., Mirmohammadsadegh, A., Walz, M., Lysa, B., Tartler, U., Remus, R., Hengge, U., Michel, G. & Ruzicka, T. (2003). *FASEB J.* **17**, 1969–1971.